

Photonic crystal nanofiber using an external grating

M. Sadgrove, R. Yalla, K.P. Nayak and K. Hakuta

Center for Photonic Innovations, The University of Electro-Communications, 1-5-1 Chofugaoka, Chofu, Japan

Compiled August 7, 2021

We implement a photonic crystal nanofiber device by reversibly combining an optical nanofiber and a nanofabricated grating. Using the finite-difference time-domain method, we design the system for minimal optical loss while tailoring the resonant wavelength and bandwidth of the device. Experimentally we demonstrate that the combined system shows a strong photonic stop-band in good agreement with numerical predictions. The resulting device may be used to realize strong light-matter coupling near to the nanofiber surface. © 2021 Optical Society of America

The realization of strong photonic confinement in micro and nano-scale dielectric structures [1] and the resultant enhancement of light-matter coupling which can be achieved near the surface of such structures has led to the current great interest in nanophotonics [2]. Within this field, photonic crystal (PhC) devices [3] in particular have shown to be a promising technology, with potential applications ranging from guided single photon emission [4] and atom trapping [5,6] to biosensing [7].

Another approach which naturally achieves the high mode confinement and strong light matter coupling associated with PhCs is that of sub-wavelength tapered optical fibers (nanofibers). High optical density and high coupling between quantum emitters and the guided-modes of a nanofiber have recently been demonstrated in such systems [8–11]. This light-matter coupling can be further enhanced by implementing a photonic crystal structure on the nanofiber [12]. Experimental realizations of such *photonic crystal nanofibers* have been achieved using ion beam etching [13] and femtosecond laser ablation techniques [14] to fabricate periodic structures on the nanofiber surface.

In this Letter, we present a new method of implementing photonic crystal properties in an optical nanofiber by combining the nanofiber with an external grating as illustrated in Fig. 1(a). Our method takes advantage of modern nanofabrication methods, which allow flexible design of planar nanostructures, in combination with nanofiber technology which produces strong transverse mode confinement and allows strong light-matter coupling and high optical densities for emitters near the nanofiber surface. The grating, which is fabricated on a silica substrate, is brought into contact with a suspended nanofiber. In the region where the nanofiber and the grating make contact, the effective refractive index experienced by the nanofiber guided mode is strongly modulated by the grating giving rise to a photonic stop-band. The stop-band along with the strong transverse mode confinement due to the nanofiber mean that the combined device may be considered to be a fiber-coupled PhC. Our device represents a new paradigm in the implementation of PhCs where two (or more) independent nano-scale optical elements may be reversibly combined

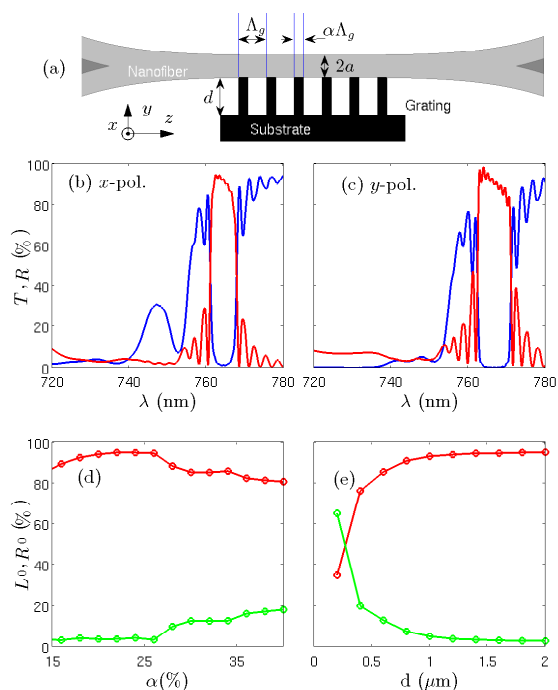


Fig. 1. (a) Experimental concept. An external grating is combined with an optical nanofiber forming a device with PhC characteristics. (b) and (c) show FDTD simulation results for the transmission T (blue line) and reflection R (red line) spectra for x and y polarizations respectively with grating parameters as defined in the main text. (d) and (e) show FDTD simulation results for the maximum reflectivity R_0 (red line) and optical loss L_0 (green line) as a function of the grating duty cycle α and the grating slat depth d respectively. In both cases, the input mode was y -polarized.

to form an effective PhC structure. Combined with a quantum dot deposited on the nanofiber surface [11] or following recent proposals for trapping single atoms in PhCs [5,6], we believe that our technique can provide a powerful and flexible tool for the realization of strong light-matter coupling with applications ranging from quantum and nano optics to biosensing.

As shown in Fig. 1(a) the external grating is defined by the following parameters: grating period Λ_g , slat width $\alpha\Lambda_g$, where α is the grating duty cycle, slat depth d and the number of slats N . Before manufacturing the grating, we simulated the system using the finite-difference time-domain (FDTD) method (Lumerical Solutions Inc.) to evaluate the optical properties of the device. In particular, in order to keep the optical loss to a minimum, it was necessary to carefully evaluate different duty cycles α and slat depths d for the grating using simulations. Although a larger duty cycle produces stronger index modulation, and thus stronger reflectivity in the stop-band, it also allows more coupling to the silica substrate and thus greater optical loss. Likewise, a shallower grating is easier to manufacture, but if the grating is too shallow, the evanescent field extending from the nanofiber can couple to the silica substrate leading to large losses. Figures 1(b) and (c) show reflection and transmission spectra from FDTD simulations for a nanofiber diameter of $2a = 625$ nm and an external grating with period $\Lambda_g = 305$ nm, duty cycle $\alpha = 25\%$, grating depth $d = 2$ μm and $N = 200$ slats.

Two orthogonal polarizations x and y were tested, with the x and y directions as defined in Fig. 1(a). For both polarizations, a strong photonic stop-band is seen in the transmission spectrum near 765 nm accompanied by a peak in the reflection spectrum. The device is seen to be lossy below a wavelength of ~ 760 nm. Denoting by λ_0 the wavelength at which the maximum reflection occurs (i.e. the *working wavelength* of the device), we can define R_0 and T_0 , the reflectivity and transmission at λ_0 respectively. The optical loss at the working wavelength is then $L_0 = 1 - R_0 - T_0$. For the x polarization, we have $\lambda_0 = 762$ nm and $R_0 = 95\%$ and the reflection spectrum full-width at half-maximum (FWHM) is $\sigma_R = 7$ nm. T_0 and L_0 are found to be 1% and 4% respectively. For the y polarization we find $R_0 = 98\%$ and $\sigma_R = 9$ nm, with $T_0 < 0.1\%$ and $L_0 = 2\%$. We note that the polarization dependence of the device is not very pronounced, with similar stop-bandwidths and peak reflectivities seen for both polarizations.

To optimize the optical properties of the device, we performed parameter sweeps over α and d in our FDTD simulations. Figures 1(d) and (e) show the results for L_0 and R_0 as functions of α and d respectively for grating and fiber parameters as given above. For the duty cycle sweep, we set $d = 2$ μm , and for the depth sweep we set $\alpha = 25\%$ and the input mode was y -polarized in both cases. As can be seen in Fig. 1(d), above $\alpha = 25\%$, a relatively sharp increase in loss is observed, and indeed we found that the loss behaviour at higher α displayed more complex characteristics as a function of the input wavelength λ . One possible reason for the loss behaviour above $\alpha = 25\%$ is the waveguide properties of the slats themselves. Clearly, as the slat width $\alpha\Lambda_g$ increases, the number of modes which can couple to the slats becomes larger leading to more complicated loss behavior. On the other hand, in Fig. 1(e) it may be seen that the loss

decreases smoothly as a function of d , falling to $L_0 = 2\%$ at $d = 2$ μm . After finding the optimum parameters for

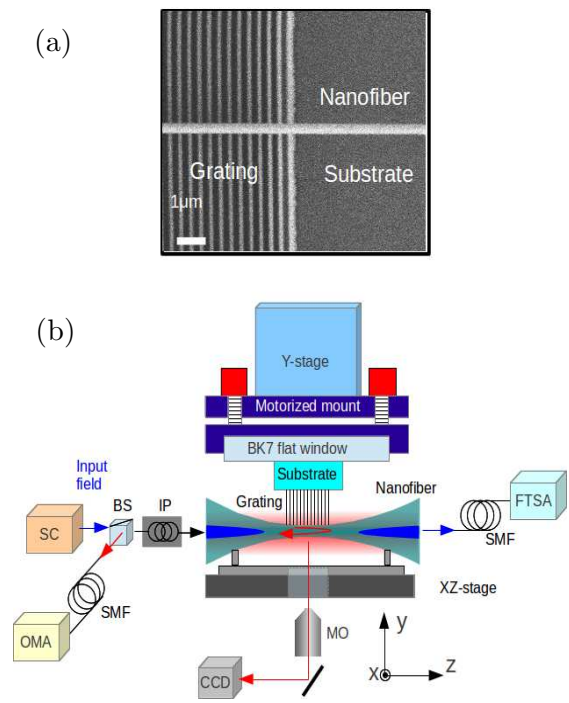


Fig. 2. (a) SEM image of the device clearly showing the grating and substrate regions along with the nanofiber. (b) Schematic diagram of the experimental setup. Light from a super-continuum source (SC) is coupled into the nanofiber which is fixed on an XZ-stage mounted on an inverted microscope. The output transmission and reflection spectra are measured by a Fourier transform spectrum analyzer (FTSA) and an optical multichannel analyzer (OMA) respectively. A full explanation of all the symbols is provided in the text.

α and d , a similar optimization procedure was used to choose N , with $N = 200$ found to be optimal. These results demonstrate that an external grating can be used to induce a photonic stop-band in a nanofiber with high reflectivity ($R_0 > 95\%$) and with optical loss as low as 2% for the parameters considered here.

For the experiments, we used a 200 slat, square grating pattern with a nominal period of 320 nm and a duty cycle of 25% fabricated on a 10 mm \times 25 mm silica substrate of thickness 2 mm (fabricated by Nanoeff Consultant Ltd.). The grating pattern extended $d = 2$ μm from the surface of the silica substrate. Figure 2(a) shows a scanning electron microscope (SEM) image of the grating with a 570 nm diameter nanofiber mounted on it.

The experimental setup is illustrated in Fig. 2(b). The grating substrate was attached to a one inch diameter optically flat BK7 window using an adhesive. The mounted grating was then inserted into a high resolution, motor-

ized mirror mount (Newfocus Picomotor 8884) so that its tilt could be precisely controlled. The motorized mount was attached to a vertical translation stage (Y-stage) (Kohzu XD2000) with 250 nm resolution. So mounted, the grating could be lowered onto the nanofiber sample with high precision. The nanofiber itself was mounted on a two-axis translation stage (XZ-stage) (Sigma Koki BIOS 305T) with a resolution of 50 nm to allow adjustment of the relative centers of the grating and the nanofiber. The XZ-stage and the Y-stage were mounted on an inverted microscope (Nikon Eclipse Ti-U). The whole experiment took place in a clean booth to avoid dust deposition on the grating and nanofiber.

For characterization of the device’s optical properties we used an optical setup as described below. The input to the nanofiber was derived from a filtered super-continuum light source (SC) (NKT Photonics SuperK EXR15). The filtered spectrum spanned from 700-1000 nm and the light was passed through a polarizing beam-splitter to ensure linear polarization. The polarization angle of the input light was controlled by an inline polarizer (IP) (Thorlabs FPC030). The transmission and reflection spectra were measured by a Fourier transform spectrum analyzer (FTSA) (Thermo Fisher Scientific Nicolet 8700) with a resolution of 0.01 nm, and an optical multichannel analyzer (OMA) (Ocean optics QE65000) with resolution 2 nm respectively. We also monitored the nanofiber/grating interface using the microscope’s 40x objective lens (MO) which focused an image of the device to a charge coupled device (CCD) camera.

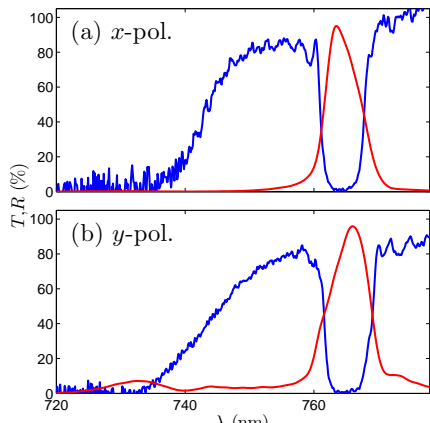


Fig. 3. (a) and (b) show experimentally measured transmission (blue line) and reflection (red line) spectra for the grating placed near the nanofiber center (nominal nanofiber diameter 570 nm) for x and y polarized light respectively.

Before bringing the grating into contact with the nanofiber, we measured the tilt of the nanofiber with respect to the horizontal using the microscope. We then adjusted the offset of the precision motorized mount so that the grating tilt matched that of the nanofiber. Finally, we used the vertical translation stage to bring the

grating close to the nanofiber. Optical contact between the grating and the nanofiber was marked by the appearance of scattered light at the nanofiber surface (as seen on the CCD camera). From this point, successful mounting of the grating on the nanofiber was accomplished by fine adjustments to the Y-stage position while monitoring the signals of the FTSA and OMA.

Figures 3(a) and (b) show measured transmission and reflection spectra for two orthogonal polarizations for a nanofiber diameter of 570 nm. We see a strong optical stop-band in the transmission spectrum at a wavelength of 765 nm accompanied by a peak in the spectrum of the reflected light occurring at $\lambda_0 = 764$ nm and 766 nm for the x and y polarizations respectively. We measured the bandwidth σ_R for the reflection spectra shown in Figs. 3(a) and (b) and found $\sigma_R = 6$ nm for the x polarization and $\sigma_R = 7$ nm for the y polarization. The optical loss is seen to become large below $\lambda \sim 750$ nm.

In order to calibrate R_0 , T_0 and L_0 for the experimental spectra, we replaced the super-continuum light source with a Titanium Sapphire laser source (Coherent MBR 110, linewidth < 75 kHz) and measured the reflected and transmitted power through the system at λ_0 and several other wavelengths within and just outside the optical stop-band. Five measurements were made at each wavelength both with and without the grating touching the nanofiber. The calibrated spectrum for the x polarization was found to have a maximum reflection $R_0 = (96 \pm 1)\%$, while for the y polarization we found $R_0 = (95 \pm 4)\%$. For both polarizations, the transmission T_0 at the peak reflective wavelength was less than 0.1% giving losses of $L_0 = (4 \pm 1)\%$ and $L_0 = (5 \pm 4)\%$ for the x and y polarizations respectively. For all values, the given errors are the standard deviation over five measurements.

We see good qualitative agreement between experimental results and the spectra calculated using FDTD numerical simulations. The quantitative values of the maximum reflectivity R_0 and σ_R are also in fair agreement between simulations and the experimental spectra as are the values of L_0 and T_0 . Additionally, both simulation and experimental results show the same lossy region for wavelengths below 750 nm. In order to reproduce both the qualitative loss characteristics and the resonant wavelength and bandwidth of the experimental spectra, it was necessary to use a grating period of $\Lambda_g = 305$ nm and a nanofiber diameter of $2a = 625$ nm in the simulations. The difference between these parameters and the nominal experimental parameters is not yet fully understood. However, we note that the experimental values were determined by SEM measurements which have an error of $\pm 10\%$. The values used in the simulations lie within this error range.

We also tested the dependence of the resonant wavelength on the diameter of the nanofiber by placing the grating at various positions along the nanofiber ($z = 0$ corresponds to the thinnest part of the nanofiber where $2a = 550$ nm). The results are shown in Figs. 4 (a) and (b). The resonant peak position λ_0 is seen to shift to the

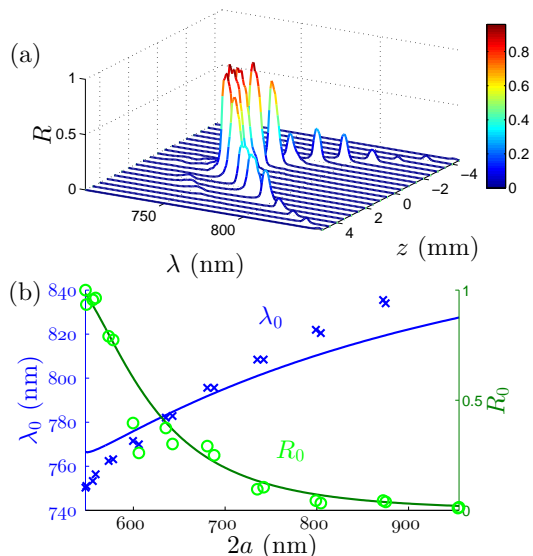


Fig. 4. In (a), reflection spectra taken at a number of different z values are shown. (b) shows the peak reflection wavelength (blue crosses) λ_0 and the peak height R_0 (green circles) as a function of the nanofiber diameter $2a$. The predictions of coupled mode theory are shown for λ_0 by a solid blue line and for R_0 by a solid green line.

red in proportion to the change in nanofiber diameter. The falloff of the reflection peak height R_0 as a increases (green circles, Fig. 4(b)) is due to the reduction in the effective index modulation at thicker diameter.

It is meaningful to evaluate our device using the coupled mode theory (CMT) [15] of fiber Bragg gratings. If we model the the index modulation by a sinusoidal variation $n = n_0 + \Delta n \sin^2[(\pi/\Lambda_g)z]$, where n_0 is the unperturbed refractive index of the core and Δn is the modulation amplitude, CMT gives $\lambda_0 = \lambda_D(1 + \Delta n/2)$, where $\lambda_D = 2n_{\text{eff}}\Lambda_g$, with n_{eff} the effective refractive index seen by the nanofiber guided mode. The peak reflection value is given by $R_0 = \tanh^2(2\pi\Delta nN\Lambda_g/\lambda_0)$. We evaluated Δn empirically by fitting the CMT theory to our experimental results, assuming the same parameters as used in the FDTD simulations. Δn was found to have a maximum of 1.1% at $2a = 550$ nm and dropped to almost 0 at $2a = 950$ nm. Since n_{eff} increases as the core diameter gets larger, λ_0 is expected to move to the red as shown by the solid blue line in Fig. 4(b), while R_0 decreases as shown by the solid green line in Fig. 4(b). It may be seen that the essential experimental features are reproduced, indicating that CMT is a useful tool for the proto-design of the device.

Our device may also be considered to be a 1D PhC waveguide. It is well known that for a quantum emitter placed near to such a waveguide, Purcell enhancement of emission into the guided modes of the waveguide is expected [4]. We have performed preliminary FDTD simulations which suggest a Purcell factor of order 10 is

possible for the device introduced here. Corresponding coupling to the guided modes of the nanofiber is then expected to be more than 60%. In addition, engineering a sub-wavelength dimension cavity in the grating pattern is another method to enhance coupling between a quantum emitter and the nanofiber guided modes. Such a structure can create a strong cavity mode at the center of the stop-band in a way analogous to “defect-mode” cavities used in distributed feedback lasers [16]. We note that for a quantum dot deposited on the nanofiber as in Ref. [11], the Purcell enhancement can be optimized by adjusting the relative position of the grating and the nanofiber which is an advantage of our method.

The present work demonstrates that PhC structures with low optical loss can be made by combining two separate nano-scale optical elements. The combined device is a PhC nanofiber with high transverse mode confinement due to the nanofiber and a stop-band due to the external grating. With suitable parameter choices, it should be possible to use the device to realize strong light-matter coupling between the nanofiber guided modes and quantum emitters.

We would like to thank Pengfei Zhang for useful discussions. This work was supported by the Japan Science and Technology Agency (JST) as one of the Strategic Innovation projects.

References

1. K.J. Vahala, Nature **424**, 839 (2003).
2. L. Novotny and B. Hecht, “Principles of nanophotonics”, Cambridge University Press (2012).
3. J. D. Joannopoulos, S. G. Johnson, J. N. Winn, and R. D. Meade, “Photonic Crystals: Molding the Flow of Light (second edition)”, Princeton University Press (2008).
4. V. S. C. Manga Rao and S. Hughes, Phys. Rev. Lett. **99**, 193901 (2007).
5. C.-L. Hung, S. M. Meenhanm D.E. Chang, O. Painter, and H.J. Kimble, arxiv:1301:5252.
6. E. Kuznetsova, J. Feist, Q. Quan, J. D. Thompson, T. Tiecke, S. F. Yelin, and M. D. Lukin, arXiv:1301.4559.
7. Y.-F. Chen, X. Serey, R. Sarkar, P. Cheng, and D. Erickson, Nanoletters **12**, 1633 (2012).
8. K.P. Nayak and K. Hakuta, New J. Phys. **10** 053003 (2008).
9. E. Vetsch, D. Reitz, G. Sagu, R. Schmidt, S. T. Dawkins, and A. Rauschenbeutel Phys. Rev. Lett. **104**, 203603 (2010).
10. A. Goban, K. S. Choi, D. J. Alton, D. Ding, C. Lacrote, M. Pototschnig, T. Thiele, N. P. Stern, and H. J. Kimble, Phys. Rev Lett. **109**, 033603 (2012).
11. R. Yalla, F. Le Kien, M. Morinaga, and K. Hakuta, Phys. Rev. Lett. **109**, 063602 (2012).
12. F. Le Kien and K Hakuta, Phys. Rev. A **80**, 053826 (2009).
13. K. P. Nayak, et al., Opt. Express **19**, 14040 (2011).
14. K.P. Nayak and K. Hakuta, Opt. Express **21**, 2480 (2013).

15. T. Erdogan "Fiber grating spectra", J. Lightwave Tech. **15**, 1277 (1997).
16. O. Painter, R. K. Lee, A. Scherer, A. Yariv, J. D. O'Brien, P. D. Dapkus, and I. Kim , Science **284**, 1819 (1999).